MATERIALS PHYSICS AND MECHANICS RESEARCH ARTICLE

Submitted: October 15, 2025 **Revised: November 11, 2025** **Accepted: November 20, 2025**

Temperature dependence of linear fracture mechanics parameters in ceramics: a finite element study

Yu.V. Ermolaeva [1], S.A. Krasnitckii [2]✉, M.Yu. Gutkin [1]

[1] Institute for Problems in Mechanical Engineering, Russian Academy of Sciences, St. Petersburg, Russia

[2] ITMO University, St. Petersburg, Russia

✉ krasnitsky@inbox.ru

ABSTRACT

Parametric finite element simulations are conducted to investigate the steady-state growth of a crack in ceramic material under various temperature conditions. The temperature dependences of elastic moduli and specific surface energy are incorporated to compute the critical fracture parameters such as the crack length, the failure stress and the energy release rate. The finite element modelling is first verified against Griffith's theory and then implemented to practical case of cracks growing from a pore. It is demonstrated that crack growth can be energetically favorable at elevated temperatures, whereas it can be inhibited at low temperatures.

KEYWORDS

high-temperature ceramics • cracks • pores • linear fracture mechanics • finite element method

Funding. *This work was supported by the Russian Science Foundation (grant No. 23-19-00236).*

Citation: Ermolaeva YuV, Krasnitckii SA, Gutkin MYu. Temperature dependence of linear fracture mechanics parameters in ceramics: a finite element study. *Materials Physics and Mechanics*. 2025;53(6): 1–11. http://dx.doi.org/10.18149/MPM.5362025_1

Introduction

The exceptional mechanical properties of ceramic materials, such as high strength, hardness, and wear resistance at elevated temperatures, make them perfect candidates for applications in extreme environments, including aerospace, energy, and manufacturing industries [1–3]. However, the widespread use of structural ceramics is often limited by their inherent brittleness and sensitivity to fracture associated with the presence of intrinsic microstructural defects introduced during manufacturing [4,5]. Among these defects, pores being one of the most common stress concentrators are effective sites for crack nucleation [6,7].

The fracture behavior of ceramics is strongly dependent on the operating temperature [8,9]. At lower temperatures, the material exhibits classic brittle fracture, where crack propagation is the dominant relaxation mechanism. In contrast, at elevated temperatures, the activation of dislocation and grain boundary (GB) sliding can induce a brittle-to-ductile transition (BDT), often accompanied by crack-tip blunting, which significantly enhances fracture toughness [10]. This transition is critical for determining the service limits and reliability of ceramic components. The problem of BDT has been extensively studied in the literature, with numerous works focused on the critical conditions of GB dislocation emission [11–14], the toughening effect of crack blunting [15–17], GB sliding [18–20] and GB segregations [21–23]. Nevertheless, a comprehensive analysis

Publisher: Peter the Great St. Petersburg Polytechnic University

linking the temperature-induced evolution of material parameters to the critical conditions for crack growth from specific defects, such as pores, remains an essential issue.

In our previous research, we have systematically investigated stress concentration and fracture initiation in ceramic composites. We analyzed local stress distributions near pores and inclusions using both analytical perturbation techniques and finite element (FE) simulations [24,25]. Furthermore, we employed FE modeling to reveal the energetical favorability of various crack configurations near lamellar inhomogeneities [26] and to study the competition between brittle and ductile fracture behavior at elevated temperatures [27].

In the present work, the effect of operating temperature on the crack tolerance of α-Al_2O_3 ceramics is investigated to assess the energy favorability of the following different fracture scenarios: (i) the homogenous scenario of crack growth without any extra source of stress disturbance, and (ii) the heterogeneous scenario of crack growth accelerated by stress concentration around a circular pore. The first scenario can be attributed to fracture initiated inside the grains (transgranular fracture), while the second scenario is addressed to intergranular fracture initiated by pre-existing defects at GBs. Some empirical temperature dependences of α-Al_2O_3 ceramics properties are involved in FE analysis in assumption of the steady-state crack growth. The elastic response of an FE model containing flaws is obtained through parametric FE simulations that account for variations in flaw lengths, applied stress and operating temperature. The resulting strain energy data are utilized to evaluate some fracture parameters including the critical crack length, the critical failure stress and the energy release rate. The validity of FE data is proved by comparison with the results of Grifith's theory for the homogeneous scenario. The obtained results allow to assess the deterioration in fracture tolerance in ceramics due to temperature rise and presence of pores as well.

Model

We consider a ceramic material subjected to a remote tensile load S under the plane strain condition. The material response is supposed to be linearly elastic and isotropic defined by the Young modulus E and the Poisson ratio ν with respect to the operating temperature T. Figure 1 illustrates two possible scenarios of crack generation in polycrystal material: (i) homogenous crack nucleation (HmCN) inside a grain with no stress concentration effect; (ii) heterogeneous crack nucleation (HtCN) initiated by the stress concentration induced by such a manufacturing defect as a circular pore of radius R_0 located at a GB.

The favorability of these scenarios can be analyzed within the framework of linear elastic fracture mechanics (LEFM) considering the following parameters: the critical crack length L_{cr}, the critical stress for crack growth S_{cr} and the energy release rate G due to the crack advance. According to Griffith's theory [10], the total energy change due to crack formation is given by the sum:

$$\Delta W = \Delta W_{st} + \Delta W_{sf}, \quad (1)$$

where ΔW_{st} is the change in the strain energy of the body and ΔW_{sf} is the energy to create new free surfaces.

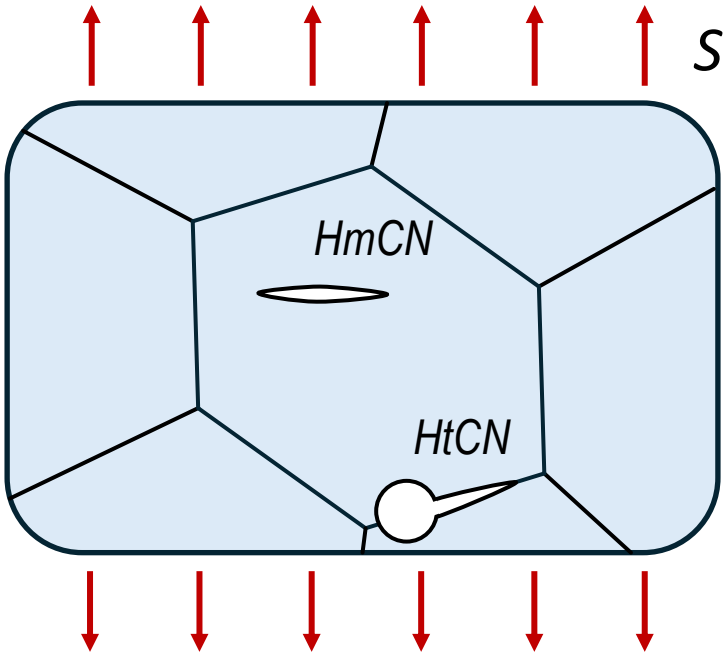

Fig. 1. Typical fracture scenarios in a polycrystalline ceramics: a transgranular crack under the homogenous stress condition (HmCN) and an intergranular crack under the heterogeneous stress condition induced by a GB pore (HtCN)

In the case of HmCN, the strain energy change due to a crack of length L (per unit length of the crack in the direction normal to Fig. 1 plane) is:

$$\Delta W_{st} = -\frac{\pi}{4}\frac{1-\nu^2}{E}L^2S^2. \quad (2)$$

The surface energy term reads:

$$\Delta W_{st} = 2L\gamma, \quad (3)$$

where γ is the specific surface energy of the ceramics.

It is supposed that a crack becomes unstable under a constant applied stress S if the crack length exceeds some critical value L_{cr} defined by the following equilibrium criteria:

$$\frac{d}{dL}\Delta W|_{S=const} = 0, \quad \frac{d^2}{dL^2}\Delta W|_{S=const} \leq 0. \quad (4a,b)$$

For instance, the critical crack length L_{cr} determined from Eqs. (4) in the case of HmCN is well-known and given by:

$$L_{cr} = \frac{4}{\pi}\frac{E\gamma}{(1-\nu^2)S^2}. \quad (5)$$

Unlike the equilibrium criteria given by Eqs. (4), the negative energy change ($\Delta W < 0$) accompanied by crack advance is considered as an alternative fracture criterion to obtain the critical parameters. For instance, the threshold stress S_{cr} can be determined from the critical condition:

$$\Delta W|_{L=const} = 0. \quad (6)$$

Substituting Eqs. (1–3) in Eq. (6), one obtains the following expression for the critical stress in the case of HmCN:

$$S_{cr} = \sqrt{\frac{8}{\pi}\frac{E\gamma}{(1-\nu^2)L}}. \quad (7)$$

It is worth noting that the value of the critical stress determined by Eq. (7) is overestimated in comparison with the one prescribed by Griffith's theory [10]. In the present work, the critical condition given by Eq. (6) is employed because it qualitatively reflects the physical aspects of fracture process. Besides, it is more adaptable to evaluate the critical values of stress from FE numerical data.

Another key parameter of fracture mechanics is the energy release rate G defined as the energy available for a crack advance. In the case of displacement-controlled loading (where the work done by an external force is zero), the energy release rate can be figured out from the expression:

$$G = -\frac{dW_{st}}{dL}, \quad (8)$$

whence for the HmCN scenario one can obtain G with respect to Eq. (2):

$$G = \frac{1-\nu^2}{E} {K_1}^2, \quad (9)$$

where K_1 is the stress intensity factor of the crack-tip, so that $K_1 = S\sqrt{\pi L/2}$. In contrast to the temperature independent parameter K_1, the energy release rate G can be strongly affected by the temperature conditions as the elastic moduli depend on the operating temperature.

Along with the analytical approach, FE simulations can be employed to evaluate the critical fracture parameters. FE method is particularly useful for studying objects with complex geometry, as is the case with HtCN where the strict analytical solution is not feasible [28]. Furthermore, standard post-processing modules in commercial FE software readily provide the values of the strain energy for the entire model. In addition, pre-processing operations directly allow to input the temperature dependences for elastic moduli.

To investigate the energy favorability of the HmCN and HtCN fracture scenarios with respect to temperature conditions, the parametric FE simulations were conducted. For this purpose, FE models comprising four-node plane strain elements were created using

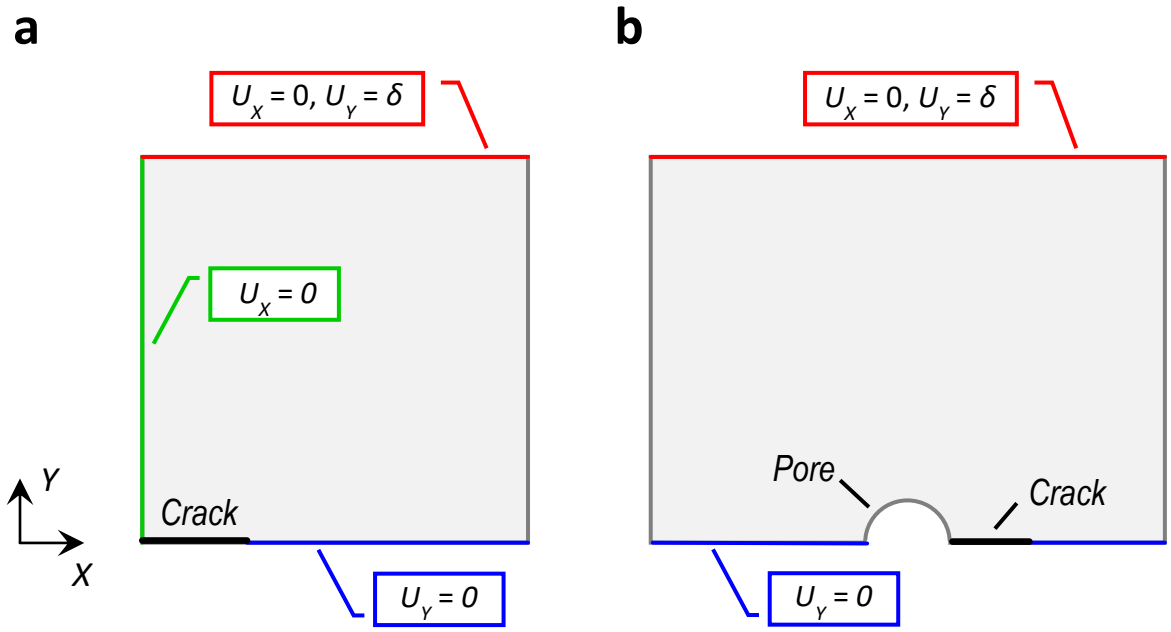

Fig. 2. The kinematic boundary conditions implemented in FE analysis of (a) homogenous crack nucleation (HmCN), and (b) heterogeneous crack nucleation (HtCN) initiated by the circular pore

ANSYS Academic Research software. Each node had two degrees of freedom corresponding to node-displacements U_X and U_Y. Figure 2 depicts the boundary conditions applied to the model with respect to the geometry and loading symmetry. The loading was assumed to be displacement-controlled by the prescribing displacement δ. The associated value of the remote stress S was subsequently calculated from the model's force reaction. The crack was treated as a flat cut with free surfaces. The model size was supposed to be an order of magnitude larger than those of both the pore and crack to eliminate boundary effects on the crack-tip stress field. For instance, the considered FE model has a size of ~ 1 μm, the average size of element in the vicinity of crack and pore is ~ 1 nm.

Since the elastic properties of corundum ceramic (α-Al_2O_3) are well-established in the literature for a wide temperature range, they were adopted to define the material behavior in the models. The following empirical approximation from [29] valid up to 1400 °C was employed in the simulations:

$$E\,[\text{GPa}] = 417 - 0.0525\,T\,[^\circ\text{C}]. \quad (10)$$

The Poisson ratio was taken as $\nu = 0.23$, as its dependence on temperature is negligible. It is worth mentioning that the FE model considers neither anisotropy of mechanical properties nor plastic response of materials. These limitations should be an issue of further investigations.

For the subsequent calculations, the temperature dependence of the specific surface energy had to be taken into account. Based on experimental data for α-Al_2O_3 ceramics [30], the following linear approximation was used:

$$\gamma = \gamma_0 - \beta T, \quad (11)$$

where the temperature T is given in K, $\beta \approx 0.83$ mJ/(m^2 K) and $\gamma_0 \approx 2138$ mJ/m^2.

Results

The parametric FE simulations considering the variations in the crack length L, the rigid displacement δ and the operating temperature T were employed to compute the change in the strain energy, $\Delta W_{st} = \Delta W_{st}|_{L>0} - \Delta W_{st}|_{L=0}$, due to both the HmCN and HtCN scenarios in the α-Al_2O_3 ceramic. The corresponding total energy change of the systems was evaluated using Eq. (1), where the strain energy term was obtained via FE modeling, while the surface energy term was determined by Eq. (3).

Figure 3 illustrates the obtained profiles of the total energy change $\Delta W(L)$ under the remote stress $S = 2.8$ GPa given for the HmCN and HtCN scenarios undergoing the temperature conditions $T = 300$ °C (Fig. 3(a)) and 1000 °C (Fig. 3(b)). One can note that the higher the temperature the lower the energy-consumption for crack growth in both scenarios. Besides, the energy values are significantly affected by the occurrence of pore. For instance, in the case of HmCN under 300 and 1000 °C the energy barriers ~ 1.2 and ~ 0.5 keV/nm should be surmounted, respectively. As for the case of HtCN, the energy barriers are significantly lower: ~ 0.3 keV/nm at 300 °C and ~ 0.1 keV/nm at 1000 °C. It is worth mentioning that the curves in Fig. 3 obtained analytically within Griffith's theory practically coincide with those computed for HmCN via FE simulations.

The maxima on the energy curves in Fig. 3 correspond to the cracks with the critical size above which the crack growth is facilitated by energy relief. The critical crack length

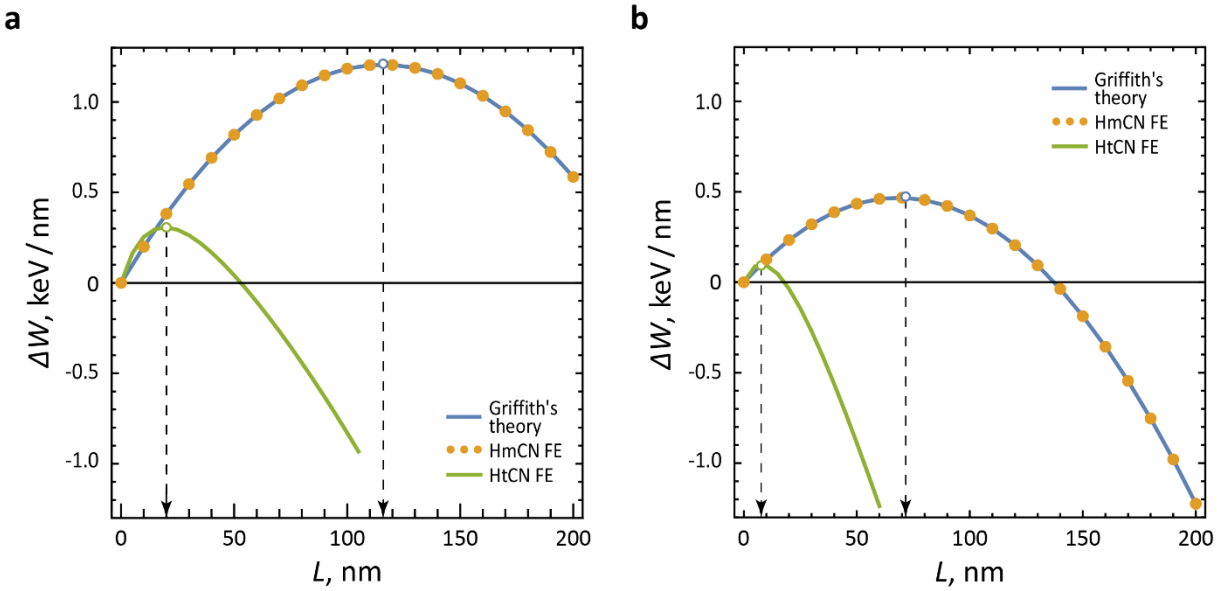

Fig. 3. Dependences of the total energy change ΔW on the crack length L given for the remote stress S = 2.8 GPa and the two operating temperatures, T = 300 °C (a) and 1000 °C (b). The curves were obtained analytically by Eqs. (1–3) (Griffith's theory) and numerically for the scenarios of homogeneous crack nucleation (HmCN FE) and heterogeneous crack nucleation initiated by the pore of radius R_0 = 100 nm (HtCN FE)

obtained by FE modeling is in good agreement with theoretical results. For example, the critical crack length indicated from the HmCN FE data in Fig. 3(a) is approximately 121 nm, that is about 4 % greater than the value ~ 116 nm prescribed by Griffith's theory.

The effect of temperature on the critical crack length is depicted in Fig. 4 for different values of the remote stress S = 2.8 and 3.6 GPa. The data reveal that L_{cr} almost linearly decreases with temperature rise in both the HmCN and HtCN scenarios. This graph can be employed to define the threshold temperature as well. In the case of HmCN under remote stress S = 2.8 GPa, the critical crack length 90 nm corresponds to

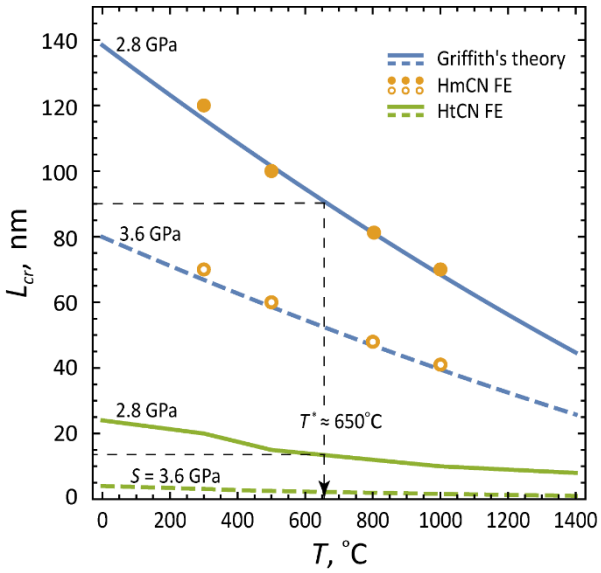

Fig. 4. Dependences of the crack critical length L_{cr} on the operating temperature T under the remote stress S = 2.8 GPa (solid curves and solid circles) and 3.6 GPa (dashed curves and hollow circles). The data were obtained analytically by Eq. (5) (Griffith's theory) and numerically for the scenarios of homogeneous crack nucleation (HmCN FE) and heterogeneous crack nucleation initiated by the pore of radius R_0 = 100 nm (HtCN FE)

the threshold temperature T^* approximately 650 °C. It means that the cracks with L = 90 nm are expected to be energetically stable if the operating temperature is lower than the threshold one ($T \leq T^*$) whilst to easily propagate at a higher temperature ($T > T^*$). In addition, it is apparent from the data for the HtCN scenario (crack growth from a circular pore of R_0 = 100 nm) acting under the same remote stress S = 2.8 GPa, that the cracks with L > 14 nm should exhibit the unstable growth under the temperature greater than ~ 650 °C.

It is worth noting that according to estimation in [25], the cleavage stress for crack advance (theoretical strength) reaches approximately 35 GPa at 1000 °C which significantly exceeds the considered values of remote stress S = 2.8 and 3.6 GPa. However, in practical cases the dislocation sliding is expected to occur under lower stress values ~1 GPa. This issue is beyond the scope of this study.

Turning now to a critical condition for the remote stress S, the energy change profiles $\Delta W(S)$ given at operating temperatures T = 300 and 1000 °C in the frame of the HmCN and HtCN scenarios are illustrated in Fig. 5(a). In accordance with the criteria introduced in the previous section, the critical stress for crack growth is prescribed by the equation $\Delta W(S_{cr}) = 0$. As is seen from Fig. 5(a) at a fixed temperature in the unloaded state (when the remote stress vanishes, S = 0), the energy change is determined by the surface energy term (see Eqs. (1–3)) predicting the identical energy values for cracks of the same length regardless of the crack initiation scenarios (HmCN and HtCN). As the remote stress S rises, the energy change ΔW drops more rapidly for HtCN than for HmCN. For example, for L = 100 nm and T = 300 °C the critical stress S_{cr} is ~1.8 GPa in the case of HtCN, that is almost two times lower than the value ~ 4.2 GPa for HmCN. Besides, the higher the temperature T the lower the critical stress S_{cr}.

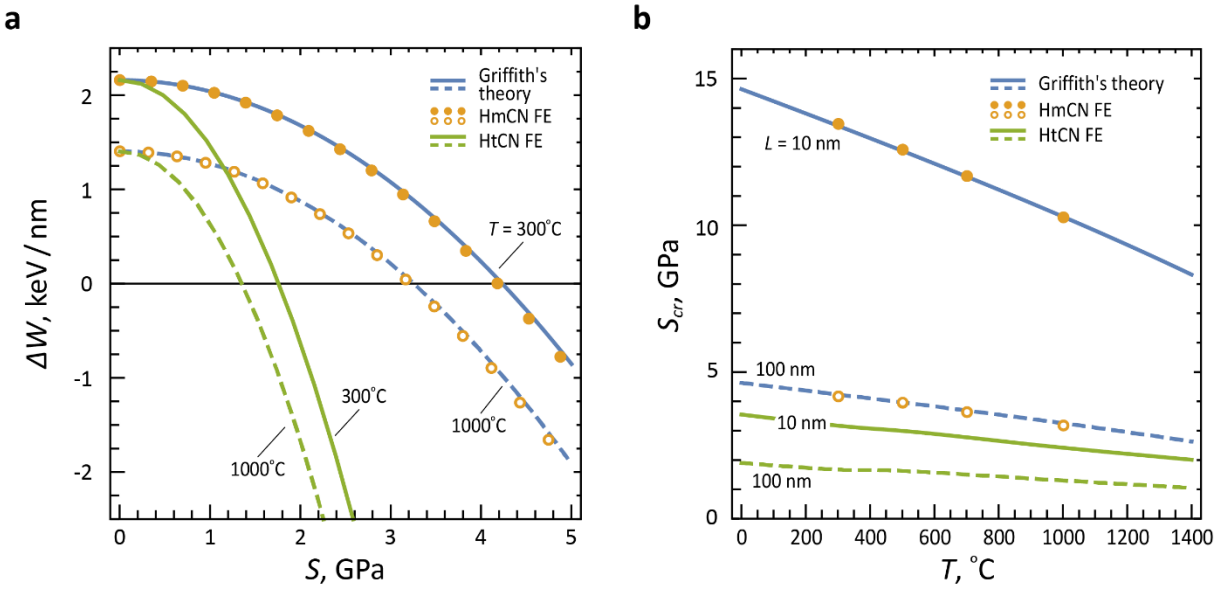

Fig. 5. (a) Dependences of the total energy change ΔW on the remote stress S given for a crack with L = 100 nm under the two operating temperatures, T = 300 °C (solid curves and solid circles) and 1000 °C (dashed curves and hollow circles). (b) Dependences of the critical remote stress S_{cr} on the operating temperature T given for cracks with L = 10 nm (solid curves and solid circles) and 100 nm (dashed curves and hollow circles). The data in (a) and (b) were obtained analytically by Eqs. (1–3,7) (Griffith's theory) and numerically for the scenarios of homogeneous crack nucleation (HmCN FE) and heterogeneous crack nucleation initiated by the pore of radius R_0 = 100 nm (HtCN FE)

The insignificant discrepancy between analytical and FE results emerges as the stress S increases (see Fig. 5(a)). Apparently, this discrepancy is caused by numerical inaccuracies accumulating due to the iterative adjustment of the displacement δ in order to maintain a constant value of the remote stress S.

Figure 5(b) demonstrates the temperature dependence of the critical stress S_{cr} provided for the crack lengths of 10 and 100 nm. What stands out from Fig. 5(b) is an approximately linear decrease of the critical stress S_{cr} with increasing T in a similar manner with the curves $L_{cr}(T)$ (see Fig. 4). In the case of HmCN, the temperature conditions remarkably affect the critical stress for relatively small cracks (L ~ 10 nm), *e.g.* $S_{cr} \approx 14$ GPa for T = 100 °C *vs.* $S_{cr} \approx 10$ GPa for T = 1000 °C. In contrast, in the case of HtCN scenario with similar small cracks (L = 10 nm) induced by a circular pore with R_0 = 100 nm, the drop is significantly less exhibited, *e.g.* $S_{cr} \approx 3.5$ GPa for T = 100 °C *vs.* $S_{cr} \approx 2.5$ GPa for T = 1000 °C. Therefore, not only does the presence of the pore lower the values of the critical stress S_{cr} but also essentially reduces its sensitivity to temperature fluctuations compared to HmCN scenario.

Further analysis of the fracture in α-Al_2O_3 ceramics concerns with computing the crack energy release rate G via FE modeling. The strain energy data obtained by FE parametric simulations can be employed to approximate the energy release rate G regarding Eq. (8) as follows:

$$G = -\frac{W_{st}|_{L+\delta L} - W_{st}|_L}{\delta L}, \tag{12}$$

where δL is the crack extension. The smaller δL utilized in numerical computations the more accurate the estimation of G by Eq. (12).

According to LEFM, the stability of a crack is defined by the value of its energy release rate G. If G is less than a critical value G_{cr} then the energy release rate is not sufficient enough to promote cracking. On the contrary, a crack tends to catastrophic grow if the inequality $G > G_{cr}$ is valid. The critical value of G directly yields from the energy criteria (Eqs. (1–4)) as $G_{cr} = 2\gamma$.

Figure 6 shows the temperature dependence of the energy release rate G for various cracks subjected to the remote stress S = 2.8 GPa. The diagrams reveal two complementary effects of the temperature increase on the fracture tolerance: an increase in the energy release rate G accelerating the growth of cracks is accompanied by a decrease in the fracture resistance G_{cr} of α-Al_2O_3 ceramics.

As it is shown in Fig. 6(a) for the HmCN scenario in the temperature range 0 < T < 1400 °C, the relatively long cracks (here with L ~ 200 nm) have a tendency to propagate since their energy release rate G is greater than the critical one, while G for relatively small cracks (here with L ~ 10 nm) is not sufficient enough to encourage their propagation. Of interest here are cracks of a middle length (here with L ~ 100 nm): as is seen, the crack growth is suppressed for T < 500 °C, whilst expected to be provided under an elevated temperature T > 500 °C.

Analogous temperature dependences of the energy release rate G are demonstrated in Fig. 6(b) for the HtCN scenario considering the generation of a crack with length of 10 nm near pores with different sizes (R_0 = 0, 10 and 100 nm). As is seen from Fig. 6(b), the presence of a pore significantly affects the value of the energy release rate for crack

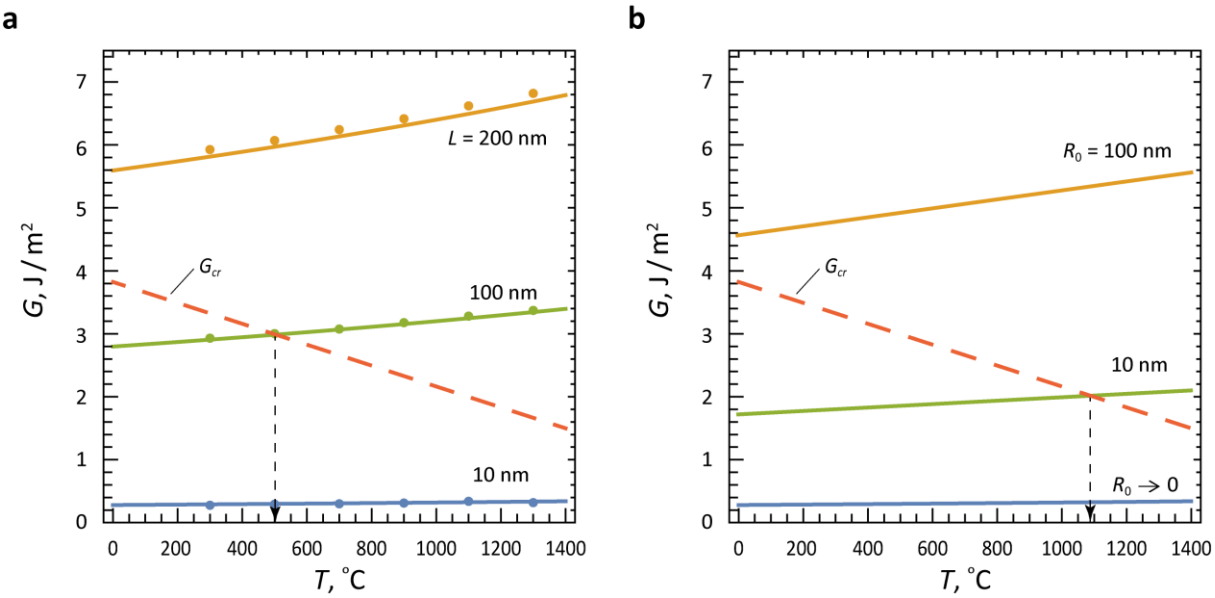

Fig. 6. Dependences of the energy release rate G on the operating temperature T under the remote stress S = 2.8 GPa in the case of (a) HmCN scenario considering the cracks of various lengths L = 10, 100 and 200 nm; here the analytical dependences given by Eq. (9) and the FE data are depicted with solid curves and circles, respectively, and (b) HtCN scenario considering a crack with L = 10 nm initiated by circular pores of different radii R_0 = 0, 10 and 100 nm. The temperature dependent critical value $G_{cr} = 2\gamma$ is given by dashed lines

advance. This effect rises with an increase in the pore radius. For instance, at the operating temperature T = 1000 °C, the energy release rate G reaches the values ~ 2 and ~ 5 J/m² for a crack initiated by a pore of the same radius as the crack length (L/R_0 = 1.0) and a pore of radius much larger than the crack length (L/R_0 = 0.1), respectively. These values are an order of magnitude higher than that for the HmCN scenario (~ 0.3 J/m² for $R_0 \to 0$). One can suggest that in the limiting case of a relatively small crack ($R_0 \gg L$), the energy release rate G tends to the value prescribed for the crack initiated at a flat surface of a semi-infinite body.

Thus, the results of FE simulations presented above clearly evidence that thermal loading and pre-existing inhomogeneities, particularly pores, are critical factors for controlling the fracture tolerance of ceramic materials.

Conclusions

In summary, the FE analysis was provided to investigate the reduction in fracture tolerance under elevated temperatures in ceramics in the frameworks of LEFM. In doing so, the linear temperature approximations of the Young module E and the specific surface energy γ was employed to compute the elastic response of FE models containing flaws and pores under remote tensile stress. The following FE models were considered: those containing a single flat flaw were utilized to describe the homogeneous nucleation of cracks (HmCN), and those considering flat flaw near a circular pore were implemented to study the heterogeneous scenario of crack nucleation accelerated by the stress concentration of inhomogeneities (HtCN). The HmCN scenario was also employed to verify the validity of the FE models against Griffith's theory. The data obtained within parametric FE simulations were used to anticipate the effect of increasing temperature

on the parameters of fracture including the critical crack length L_{cr}, the failure stress S_{cr}, the total energy change ΔW, and the rate of strain energy release G due to crack extension.

The results performed for the α-Al_2O_3 ceramics clearly demonstrate the deterioration in the fracture toughness (L_{cr}, $S_{cr}$and G_{cr}) at elevated temperatures as well as the reduction in the total energy change ΔW due to flaw generation. An opposite effect is indicated for the crack driving force, the decrease in material stiffness (the Young modulus) stimulates the rise of G as operating temperature T increases. The most obvious finding to emerge from obtained data is that the linear approximations can be employed to estimate quite accurately the aforementioned parameters with temperature change. The temperature slope of these approximations significantly depends on the crack and pore sizes, and the applied stress. The increase of these parameters drives the decrease of the temperature slope of fracture toughness criteria (L_{cr}, S_{cr}), while the temperature slope of energy release rate G increases.

CRediT authorship contribution statement

Yulia V. Ermolaeva: data curation, investigation; **Stanislav A. Krasnitckii**: conceptualization, writing – original draft; **Mikhail Yu. Gutkin**: supervision, writing – review & editing.

Conflict of interest

The authors declare that they have no conflict of interest.

References

1. Ramachandran K, Boopalan V, Bear JC, Subramani R. Multi-walled carbon nanotubes (MWCNTs)-reinforced ceramic nanocomposites for aerospace applications: a review. *Journal of Materials Science.* 2022;57(6): 3923–3953.
2. Shvydyuk KO, Nunes-Pereira J, Rodrigues FF, Silva AP. Review of ceramic composites in aeronautics and aerospace: A multifunctional approach for TPS, TBC and DBD applications. *Ceramics.* 2023;6(1): 195–230.
3. Wyatt BC, Nemani SK, Hilmas GE, Opila EJ, Anasori B. Ultra-high temperature ceramics for extreme environments. *Nature Reviews Materials.* 2024;9(11): 773–789.
4. Zhang K, Meng Q, Qu Z, He R. A review of defects in vat photopolymerization additive-manufactured ceramics: Characterization, control, and challenges. *Journal of the European Ceramic Society.* 2024;44(3): 1361–1384.
5. Gavalda-Diaz O, Saiz E, Chevalier J, Bouville F. Toughening of ceramics and ceramic composites through microstructure engineering: A review. *International Materials Reviews.* 2025;70(1): 3–30.
6. Li Z, Wang KF, Wang BL, Li JE. Size effect on the punch performance of brittle porous ceramics: theoretical analysis and numerical simulation. *International Journal of Mechanical Sciences.* 2021;207: 106674.
7. Liang C, Gao X, Fu L, Mei H, Cheng L, Zhang L. Pore evolution and mechanical response under locally varying density defects in ceramic matrix composites. *Composites Part B: Engineering.* 2024;279: 111459.
8. Jin H, Zhang S, Hao Y, Yang Y, Xu C. Mechanical properties and fracture behavior of ultrahigh temperature ceramics at ultrahigh temperatures. *Ceramics International.* 2023;49(17): 28532–28537.
9. Sheinerman AG. Model of enhanced flexural strength of ceramics at elevated temperatures. *Mechanics of Materials.* 2025;208: 105398.
10. Anderson TL. *Fracture mechanics: fundamentals and applications*. Boca Raton: CRC press; 2017.
11. Bobylev SV, Mukherjee AK, Ovidko IA. Emission of partial dislocations from amorphous intergranular boundaries in deformed nanocrystalline ceramics. *Scripta Materialia.* 2009;60(1): 36–39.

12. Zeng XH, Hartmaier A. Modeling size effects on fracture toughness by dislocation dynamics. *Acta Materialia.* 2010;58(1): 301–310.
13. Armstrong RW. Material grain size and crack size influences on cleavage fracturing. *Philosophical Transactions of the Royal Society A: Mathematical, Physical and Engineering Sciences.* 2015;373(2038): 20140124.
14. Reiser J, Hartmaier A. Elucidating the dual role of grain boundaries as dislocation sources and obstacles and its impact on toughness and brittle-to-ductile transition. *Scientific Reports.* 2020;10(1): 2739.
15. Beltz GE, Lipkin DM, Fischer LL. Role of crack blunting in ductile versus brittle response of crystalline materials. *Physical Review Letters.* 1999;82(22): 4468.
16. Fischer LL, Beltz GE. The effect of crack blunting on the competition between dislocation nucleation and cleavage. *Journal of the Mechanics and Physics of Solids.* 2001;49(3): 635–654.
17. Ovidko IA, Sheinerman AG. Grain size effect on crack blunting in nanocrystalline materials. *Scripta Materialia.* 2009:60(8): 627–630.
18. Sheinerman AG, Ovidko IA. Grain boundary sliding and nanocrack generation near crack tips in nanocrystalline metals and ceramics. *Materials Physics and Mechanics.* 2010:15(1/2); 37–46.
19. Sheinerman AG, Morozov NF, Gutkin MYu. Effect of grain boundary sliding on fracture toughness of ceramic/graphene composites. *Mechanics of Materials.* 2019;137: 103126.
20. Gutkin MYu, Krasnitckii SA, Skiba NV. Formation of liquid-like inclusions near pores in amorphous intercrystalline layers in high-temperature ceramics. *Materials Physics and Mechanics.* 2024;52(6): 8–16.
21. Sheinerman AG. Strengthening of nanocrystalline alloys by grain boundary segregations. *Materials Physics and Mechanics.* 2022;50(2): 193–199.
22. Sheinerman AG. Modeling the effect of grain boundary segregations on the fracture toughness of nanocrystalline and ultrafine-grained alloys. *Metals.* 2023;13(7): 1295.
23. Sheinerman AG, Shevchuk RE. Toughening of nanocrystalline alloys due to grain boundary segregations: finite element modeling. *Materials Physics and Mechanics.* 2023;51(7): 34–41.
24. Vakaeva AB, Krasnitckii SA, Smirnov A, Grekov, MA, Gutkin MYu. Stress concentration and distribution at triple junction pores of three-fold symmetry in ceramics. *Reviews on Advanced Materials Science.* 2018;57(1): 63–71.
25. Vakaeva AB, Krasnitckii SA, Grekov MA, Gutkin MYu. Stress field in ceramic material containing threefold symmetry inhomogeneity. *Journal of Materials Science.* 2020;55(22): 9311–9321.
26. Ignateva EV, Krasnitckii SA, Sheinerman AG, Gutkin MYu. The finite element analysis of crack tolerance in composite ceramics. *Materials Physics and Mechanics.* 2023:51(2): 21–26.
27. Krasnitckii SA, Sheinerman AG, Gutkin MYu. Brittle vs ductile fracture behavior in ceramic materials at elevated temperature. *Materials Physics and Mechanics.* 2024;52(2): 82–89.
28. Murakami Y. (Ed.) *Stress Intensity Factors Handbook. In 2 Volumes.* Oxford: Pergamon press; 1987.
29. Munro RG. Evaluated material properties for a sintered alpha-alumina. *Journal of the American Ceramic Society.* 1997;80(8): 1919–1928.
30. Weirauch DA, Ownby PD. Application of the Zisman critical surface tension technique to ceramic surfaces at high temperature. *Journal of Adhesion Science and Technology.* 1999;13(11): 1321–1330.